

# Carbon/molecule/metal molecular electronic junctions: the importance of “contacts”

Richard L. McCreery, Umamaheswari Viswanathan, Rajendra Prasad Kalakodimi and Aletha M. Nowak

Received 22nd April 2005, Accepted 24th June 2005

First published as an Advance Article on the web 23rd September 2005

DOI: 10.1039/b505684p

Molecular electronic junctions fabricated by covalent bonding onto a graphitic carbon substrate were examined with Raman spectroscopy and characterized electronically. The molecular layer was a 4.5 nm thick multilayer of nitroazobenzene (NAB), and the top contact material was varied to investigate its effect on junction behavior. A 3.0 nm thick layer of copper, TiO<sub>2</sub>, or Al(III) oxide (AlO<sub>x</sub>) was deposited on top of the NAB layer, followed by a 7.0 nm thick layer of gold. Copper “contacts” yielded molecular junctions with low resistance and showed a strong dependence on molecular structure. Carbon/NAB/AlO<sub>x</sub>/Au junctions exhibited high resistance, with current densities three orders of magnitude less than those for analogous Cu junctions. However, Raman spectroscopy revealed that the NAB layer was reduced when the carbon substrate was biased negative, to a product resembling that resulting from electrochemical reduction of NAB. Carbon/NAB/TiO<sub>2</sub>/Au junctions showed rectifying  $J/V$  behavior, with high conductivity to electrons able to enter the TiO<sub>2</sub> conduction band. Substitution of azobenzene for nitroazobenzene yielded junctions with similar spectroscopic and electronic behavior to NAB, indicating that the nitro group is not essential for rectification. The results are interpreted in terms of the energy levels of the molecule relative to those of TiO<sub>2</sub>. The combination of a covalently bonded molecular layer and a semiconducting oxide yields unusual electronic properties in a carbon/molecule/semiconductor/Au molecular junction.

## Introduction

A central goal of molecular electronics is the determination of how structure controls electron transport (ET).<sup>1–5</sup> In the case of molecular junctions of the type metal/molecule/metal, it is generally accepted that ET depends on both the structure of the molecule and the nature of the metal/molecule interface at both “contacts”.<sup>2–4,6–8</sup> For example, the conductance across a gold/thiol linkage is higher than across a noncovalent alkane/Au bond,<sup>8–11</sup> and varies significantly for Au–O, Au–S, and Au–Se linkages.<sup>12–14</sup> For an Au/thiobiphenyl/Ti molecular junction, the biphenyl/Ti contact showed Schottky behavior with temperature and bias, while the ET through the Au–S bond appeared to be controlled by a thermally activated hopping mechanism.<sup>15</sup> The temperature dependence of carbon/biphenyl/Hg junctions indicated both a tunneling process at low temperature and activated ET at higher temperature, possibly related to ring rotation.<sup>16</sup> Molecular junction paradigms based on self assembled monolayer<sup>15,17–21</sup> and Langmuir Blodgett<sup>22–27</sup> structures have quite different chemistry at the interface between the molecule and metal or metal oxide. In order to understand ET in molecular electronic junctions, it will be important to determine the contributions of the structures of both the contacts and the molecule in controlling ET, and then to integrate these contributions into rational design of molecular electronic devices.

Department of Chemistry, Ohio State University, Columbus OH 43210, USA. E-mail: McCreery.2@osu.edu

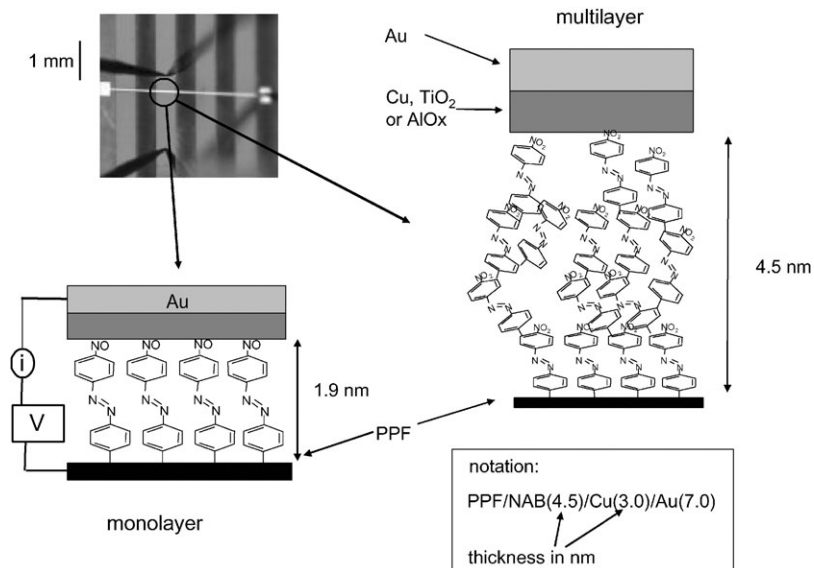


**Fig. 1** Structure of carbon/NAB/metal molecular junctions. Photograph shows the crossed-wire geometry of a metal wire on top of a carbon strip. Thicknesses of molecular and metallic layers are shown in parentheses, in nm. Metallic phase between the molecule and the gold top contact is Cu, TiO<sub>2</sub>, or Al(III) oxide.

Our laboratory has pursued a unique approach to studying molecular junctions based on a graphitic carbon substrate,<sup>16,28–34</sup> shown in Fig. 1. The primary motive for using the carbon substrate is the strong C–C bond between the molecular layer and the substrate ( $\sim 100 \text{ kcal mol}^{-1}$ ). In addition, the phenyl ring of the molecule is bonded to a phenyl ring in the graphitic “contact”, resulting in a nearly symmetric linkage with a possibly low injection barrier. The substrate is a pyrolyzed photo resist film (PPF)<sup>35,36</sup> with a structure and resistivity ( $0.005 \Omega \text{ cm}$ ) similar to glassy carbon and very flat surfaces ( $< 5 \text{ \AA}$  rms). Molecules are bonded to PPF by electrochemical reduction of diazonium reagents to yield a molecular layer, which has been characterized by Raman, XPS, FTIR, SIMS and voltammetry.<sup>33,37–45</sup> As shown in Fig. 1, diazonium modification can yield mono or multilayers, and in all cases reported here, the molecular layer thickness was verified with AFM “scratching”.<sup>46</sup> Carbon/molecule/metal junctions can be fabricated with a high device yield ( $> 80\%$ ) and 5–30% reproducibility of conductance at both low ( $\pm 0.1$ ) and high ( $\pm 2 \text{ V}$ ) applied bias.<sup>34</sup>

Given the novelty of the carbon/molecule/metal junction design, we have used a semi-empirical approach to determine what phenomena control junction conductance. We vary one aspect of the junction structure, such as molecular structure, while keeping all others constant. This approach is conceptually similar to the many structure–reactivity relationships investigated by chemists for centuries. An example is shown in Fig. 2, for PPF/molecule/Cu junctions.<sup>34</sup> The cases shown have identical PPF–molecule bonds, nearly the same molecular layer thickness (1.5–1.7 nm) and the same top contact (Cu). However, the current/voltage behavior of the three junctions varies dramatically, at both low and high bias. The ET mechanisms underlying these variations are currently under investigation, but Fig. 2 clearly establishes that molecular structure is important to junction conductance.

The current report considers variation of the top “contact” and its effect on ET through PPF/nitroazobenzene (NAB) molecular junctions. The junctions consisted of a 4.5 nm thick NAB layer on PPF, and a top contact of 3.0 nm of Cu, Ti, or Al and 7.0 nm of Au. For example, a NAB/Cu junction is designated PPF/NAB(4.5)/Cu(3.0)/Au(7.0), with the numbers in parentheses indicating layer thickness in nanometers. By varying the identity and deposition conditions for the metal or metal oxide layer between the NAB and Au, dramatic changes in junction electronic behavior were observed.

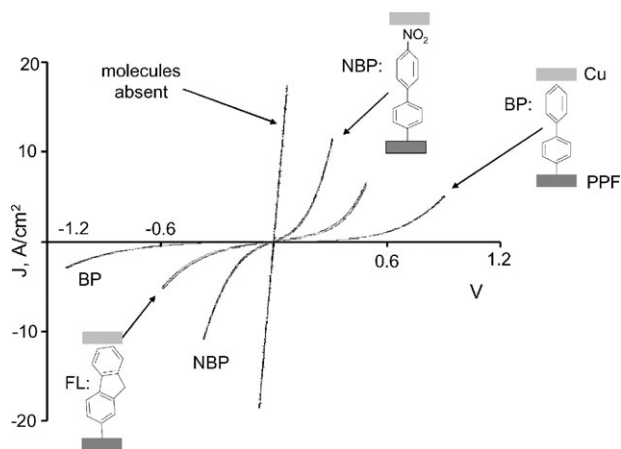


**Fig. 2** Current density vs. bias curves for three types of PPF/molecule/Cu/Au junctions, plus a “control” junction lacking the molecular layer. In all cases, the bias axis is PPF relative to Au. Scan rate was  $1000 \text{ V s}^{-1}$ . Adapted from ref. 34.

## Experimental

Molecular junctions were of the “crossed wire” type<sup>34</sup> shown in Fig. 1. The preparation of PPF and modification with NAB are described in detail elsewhere.<sup>31,34</sup> The NAB modification yields a multilayer with a thickness of  $4.51 \pm 0.68 \text{ nm}$ , as determined with AFM “scratching”.<sup>46</sup> Briefly, a series of line profiles through a trench intentionally cut in the NAB layer were averaged to determine the NAB layer depth. As shown by FTIR,<sup>37,38</sup> SIMS,<sup>39</sup> and AFM,<sup>44,46,47</sup> multilayer formation is possible during diazonium reduction by continued generation of NAB radicals and attack of the first monolayer. Although the multilayer is disordered, it is very low in pinholes and is conjugated throughout its length between PPF and the top contact. Modification of PPF occurred on 1 mm wide strips of PPF ( $\sim 1 \mu\text{m}$  thick) on  $\text{Si}_3\text{N}_4$ , with thicknesses of  $\sim 1 \mu\text{m}$ . The PPF/NAB(4.5) samples were rinsed in purified  $\text{CH}_3\text{CN}$ , then the top metal strip was deposited by electron-beam deposition with one of four programs, listed in Table 1. Ti metal was deposited with two sets of conditions, which differ significantly in their oxide composition. The Ti oxide layer formed with lower deposition pressure is referred to herein as “ $\text{TiO}_x$ ”, and that from the higher pressure with exposure of Ti to air as “ $\text{TiO}_2$ ”. XPS depth profiling showed the  $\text{TiO}_x$  deposit to be a mixture of Ti(II), Ti(III), and Ti(IV) oxyhydroxides,<sup>48</sup> while “ $\text{TiO}_2$ ” shows only Ti(IV) oxide with no detectable hydroxide.<sup>49</sup> In all cases, the Au top layer was used to protect the metal/metal oxide layer from air and to permit good electrical contact. The metal strip was 0.5 mm wide, yielding a finished junction area of  $0.005 \text{ cm}^2$ . The notation for describing junction types includes the thickness of the molecular and metal/oxide layers in nanometers, e.g. PPF/NAB(4.5)/ $\text{AlO}_x$ (3.3)/Au refers to a 4.5 nm thick NAB layer, a 3.3 nm thick  $\text{AlO}_x$  layer, and a top contact of 7.0 nm of Au.

Current–voltage ( $J/V$ ) curves were obtained conventionally using a 3-wire configuration which compensated for PPF resistance, and are plotted as current density vs. voltage (PPF relative to Au). The metal wire resistance was less than  $20 \Omega$  (determined independently) and the ohmic potential error from the metal was ignored. The  $\sim 10 \text{ nm}$  thick metal contacts are sufficiently transparent to obtain Raman spectra of the junction with a bias applied. As described elsewhere,<sup>32</sup> Raman spectra were obtained from junctions, which were identical to those studied electronically, except for a larger area ( $1 \times 7 \text{ mm}$ , or  $0.07 \text{ cm}^2$ ). An  $\text{Ar}^+$  laser (514.5 nm, 30 mw at sample) with a line focus ( $50 \mu\text{m} \times 5 \text{ mm}$ ) was the source, and an  $f/2$  spectrograph, back thinned CCD and holographic laser rejection filter detected Raman scattered light.<sup>50</sup>

**Table 1** Metal deposition conditions

PPF/Molecule/Cu (3.0)/Au (7.0)	Pressure/Torr	Rate/nm s <sup>-1</sup>
Cu (3.0 nm)	$3 \times 10^{-7}$	0.1
Au (7.0 nm)	$3 \times 10^{-7}$	0.1

PPF/Molecule/AlO <sub>x</sub> /Au		
Al (3.3 nm)	$5 \times 10^{-6}$	0.03
Au (7.0 nm)	$5 \times 10^{-6}$	0.1

PPF/Molecule/TiO <sub>x</sub> /Au		
TiO <sub>x</sub> (3.1 nm)	$< 5 \times 10^{-6}$	0.03
Au (7.0 nm)	$4 \times 10^{-6}$	0.1

PPF/Molecule/TiO <sub>2</sub> /Au		
TiO <sub>x</sub> (3.1 nm)	$7 \times 10^{-6}$	0.03
Vent with air	~760	(45 min)
Au (7.0 nm)	$4 \times 10^{-6}$	0.1

## Results

When comparing molecular junctions with varying composition, keep in mind that all junctions have the PPF/NAB(4.5) substrate and molecular layer plus the 7.0 nm Au top layer.  $J/V$  curves for PPF/NAB(4.5) junctions prepared with different top contacts are shown in Fig. 3. The Cu and TiO<sub>2</sub> junctions are relatively stable with time, with a slow increase in resistance over a period of several months. However, TiO<sub>x</sub> junctions become significantly less conductive on a timescale of hours or days. Immediately after metal deposition at low backpressure, the TiO<sub>x</sub> junctions are similar to those made with copper. As the Ti is further oxidized during or after metal deposition, the  $J/V$  curve becomes asymmetric, and rectification is observed when the Ti is present as TiO<sub>2</sub>.

Fig. 4 shows  $J/V$  curves for the Cu and TiO<sub>2</sub> junctions with a more sensitive current density scale, as well as a  $J/V$  curve for AlO<sub>x</sub> (upper panel), and a magnified AlO<sub>x</sub> curve (lower panel). Notice that the AlO<sub>x</sub> junction exhibits a symmetric  $J/V$  response with current densities more than three orders of magnitude lower than the Cu junctions. Even for voltages above +2 V, the current density for the AlO<sub>x</sub> junctions remains much lower than either the Cu or TiO<sub>2</sub> junctions.

At first glance, the reason for the dramatic difference between Cu and AlO<sub>x</sub> junctions may seem obvious. Transport in PPF/NAB(4.5)/Cu(3.0)/Au junctions relies on ET through two good conductors (PPF & Cu) and a thin, conjugated molecular layer. While there are many interesting questions about what factors control ET through the molecular layer, it is much faster for Cu junctions than for those containing AlO<sub>x</sub> or TiO<sub>2</sub>, all else being equal. AlO<sub>x</sub> is an insulator (band gap of ~8.7 eV), so it is not surprising that conductivity is blocked by a 30 Å AlO<sub>x</sub> layer. The low conductance observed in Fig. 4 for  $|V| > 2$  V may be due to field emission through the AlO<sub>x</sub> layer, or to defects.

However, the Raman spectroscopy results in Fig. 5 show that AlO<sub>x</sub> is not acting as a simple insulator in PPF/NAB(4.5)/AlO<sub>x</sub>(3.0)/Au junctions. Deposition of AlO<sub>x</sub> causes a decrease of the 1340 and 1108 cm<sup>-1</sup> Raman band intensities and an increase of the 1401/1448 cm<sup>-1</sup> intensity ratio,

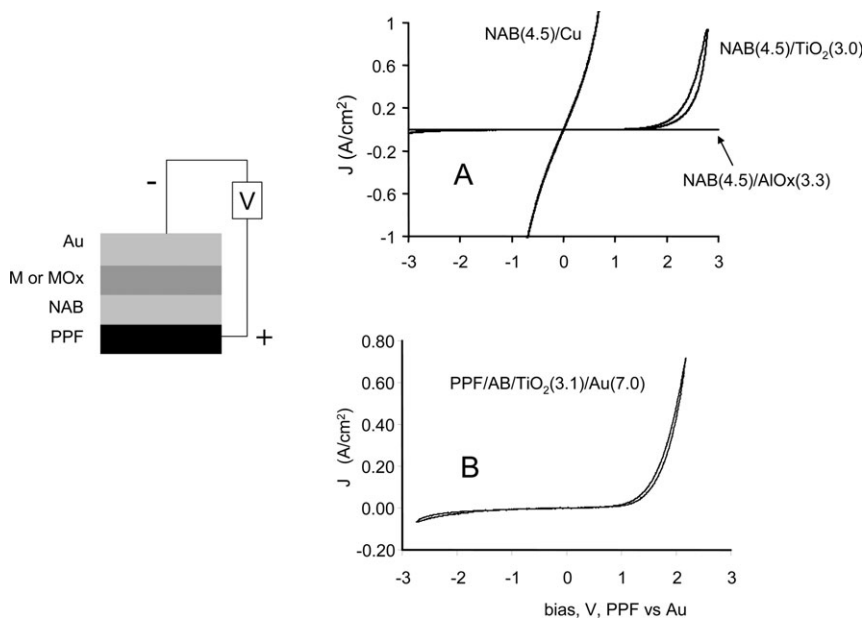


**Fig. 3** A.  $J/V$  curves for PPF/NAB(4.5) junctions which are identical except for the metal phase in contact with the NAB. Scan rate of  $100 \text{ V s}^{-1}$ . B.  $J/V$  curve for a azobenzene/ $\text{TiO}_2/\text{Au}$  junction, also at  $100 \text{ V s}^{-1}$ . AB thickness was not determined independently, but was approximately  $4 \text{ nm}$ .

as shown in the top two spectra of Fig. 5. A study of NAB in solution and NAB bonded to PPF immersed in electrolyte revealed that increases in the  $1400/1450$  peak ratio and loss of the  $1340 \text{ cm}^{-1}$  band are associated with NAB reduction to an anion or “methide” species.<sup>33,51</sup> When a negative potential is applied to a completed PPF/NAB(4.5)/ $\text{AlO}_x(3.3)/\text{Au}(7.0)$  junction, the spectra (c) to (f) shown in Fig. 5 result. For progressively negative bias (PPF negative), the  $1401/1448$  intensity ratio continues to increase. Fig. 6 compares the spectrum obtained at  $-2 \text{ V}$  to that resulting from electrochemical reduction of NAB bonded to PPF and immersed in acetonitrile electrolyte. The

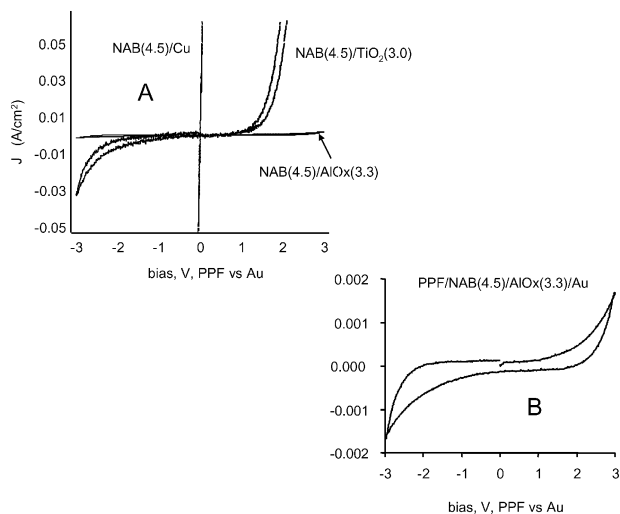


**Fig. 4** A.  $J/V$  curve of Fig. 3A with expanded current scale. B.  $J/V$  curve for PPF/NAB(4.5)/ $\text{AlO}_x(3.3)/\text{Au}$  junction after further expansion of current scale,  $100 \text{ V s}^{-1}$ .

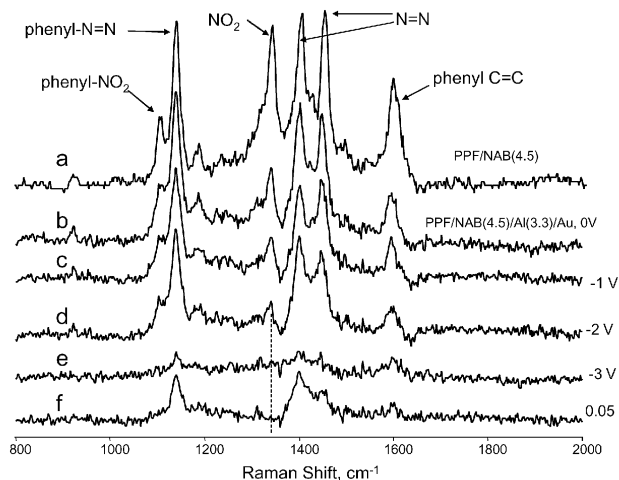


**Fig. 5** *In situ* Raman spectra of a PPF/NAB(4.5)/AlO<sub>x</sub>(3.3)/Au junction with an applied bias. Spectrum (a) is PPF/NAB(4.5) before AlO<sub>x</sub> was deposited, and (b) is after AlO<sub>x</sub> deposition without an applied bias. Remaining spectra show changes occurring when the indicated voltages were applied, progressing from top to bottom. All spectra have the same intensity scale, but are displaced vertically for clarity. Spectra (b) through (f) are from the same sample.

spectra are very similar, and the azo stretches at 1401 and 1448 cm<sup>-1</sup> resemble those of an amino substituted azobenzene also shown in Fig. 6. In fact, the Raman spectrum at -2 V in Fig. 5 is very similar to that of the electrochemically reduced NAB/PPF in which the nitro group had become an amino or hydroxylamine group. Nitro group reduction of aromatic nitro compounds is well understood, and leads to aromatic amines or hydroxylamines.<sup>52,53</sup> The details of the reaction of NAB for negative bias are under investigation, but the Raman results of Fig. 5 provide unequivocal evidence for structural changes under bias, similar to those associated with NAB reduction. Note that the current required for reduction is very small (a few μA cm<sup>-2</sup>) and much smaller than the

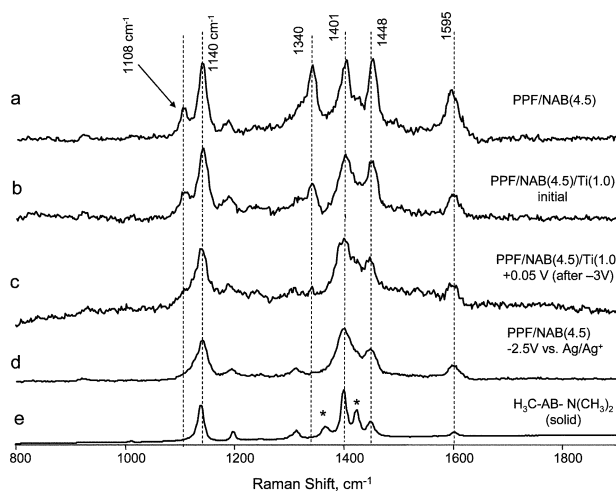


**Fig. 6** Raman spectra of PPF/NAB(4.5) before (a) and after (b) deposition of 1.0 nm of Ti and 9.0 nm of Au, and after a potential excursion to -3 V in a working junction. (c). Spectrum (d) is from a PPF/NAB(4.5) surface immersed in 0.1 M tetrabutylammonium tetrafluoroborate in acetonitrile and reduced electrochemically at -2.5 V vs. Ag/Ag<sup>+</sup>. Spectrum (e) is a Raman spectrum of *N,N*-dimethylamino-4'-methyl azobenzene, as a powdered solid. \* indicate modes attributable to the methyl groups.

capacitive or tunneling currents apparent in Fig. 4. The disappearance of the spectrum at  $-3$  V is likely due to a shift in the NAB absorption band, with accompanying decrease in resonance enhancement of the NAB bonded to PPF.<sup>49</sup>

Examination of PPF/NAB(4.5)/Cu(3.0)/Au junctions did not reveal changes in the Raman spectrum with an applied bias, although the bias range was limited due to the high currents in Cu junctions. Nevertheless, comparison of the Cu and  $\text{AlO}_x$  behavior results leads to a working hypothesis. For Cu junctions, ET is rapid through the molecular layer, leading to the high observed current density. As noted elsewhere, the  $J/V$  curves for Cu junctions are weakly temperature dependent (10–20% decrease from  $T = 313$  K to 221 K).<sup>34</sup> So neither the spectroscopy nor the temperature dependence provides evidence for a structural rearrangement in Cu junctions, although that possibility is not ruled out. With  $\text{AlO}_x$  present, however, ET through the junction is prevented and a large electric field can develop across the molecule. Even in the absence of dc current flow, the Fermi level of the PPF can be high enough under negative bias to reduce the NAB. An alternative possibility involves a very thin electrochemical cell, in which the  $\text{AlO}_x$  layer acts as an electrolyte. Under the latter hypothesis, oxidation must occur at the gold electrode, either of some junction component or of gold itself. Under either hypothesis, the  $\text{AlO}_x$  slows down ET through the junction by three orders of magnitude or more compared to Cu, and changes in molecular structure result.

$\text{TiO}_2$  is a semiconductor with a band gap of 3.0–3.4 eV, depending on phase (anatase or rutile) and disorder.<sup>54,55</sup> We might predict that a PPF/NAB(4.5)/ $\text{TiO}_2$ (3.0)/Au junction would conduct electrons with sufficient energies to enter the  $\text{TiO}_2$  conduction band. The suboxides of Ti(II) and Ti(III) are nearly as conductive as Ti metal, and about 8 orders of magnitude more conductive than  $\text{TiO}_2$ . We have shown previously Ti deposition also partially reduces NAB on PPF, with a thicker Ti layer resulting in greater reduction.<sup>32,33</sup> Fig. 7, along with our previous report,<sup>32</sup> show that the PPF/NAB/ $\text{TiO}_2$ /Au junctions exhibit spectroscopic changes under bias, qualitatively similar to those of PPF/NAB/ $\text{AlO}_x$ /Au junctions. Negative bias causes further increases in the 1401/1448 intensity ratio, and the spectrum following a negative bias excursion is similar to that of electrochemically reduced NAB. As discussed elsewhere, the spectroscopic results indicate an irreversible reduction of the nitro group to an amino or hydroxylamine which is itself electroactive.<sup>32</sup> For the present purposes, it is sufficient to conclude that NAB reduction occurs under negative bias for both PPF/NAB(4.5)/ $\text{AlO}_x$ (3.3)/Au and PPF/NAB(4.5)/ $\text{TiO}_2$ (3.0)/Au junctions.

Finally, the role of the nitro group in NAB junctions was investigated by making several junctions from azobenzene (AB). Although AB junctions have not yet been characterized extensively, PPF/AB/ $\text{TiO}_2$ (3.0)/Au junction show rectification similar to that of the analogous

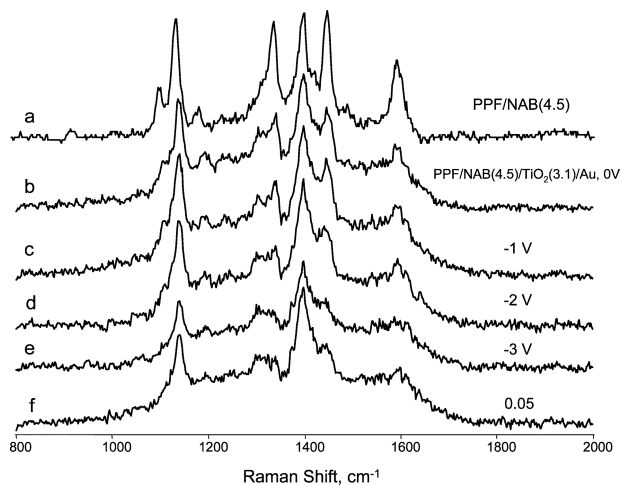


**Fig. 7** *In situ* Raman spectra of a PPF/NAB(4.5)/ $\text{TiO}_2$ (3.1)/Au junction with an applied bias. Spectrum (a) is PPF/NAB(4.5) before  $\text{TiO}_2$  was deposited, and (b) is after  $\text{TiO}_2$  deposition without an applied bias. Remaining spectra show changes occurring when the indicated voltages were applied. Spectra b–f were obtained in the sequence shown from a single sample, and all spectra have the same intensity scale.

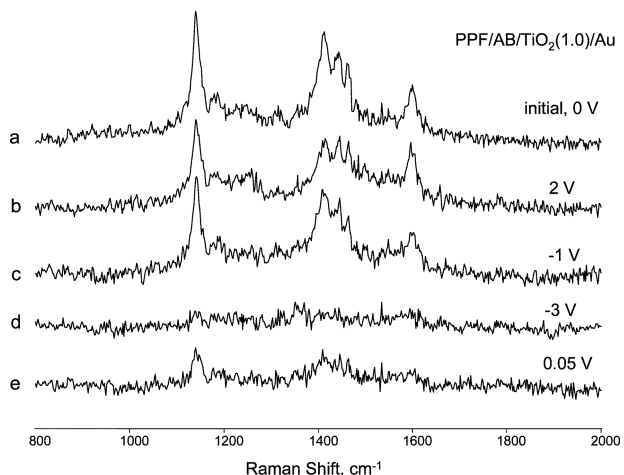


**Fig. 8** *In situ* Raman spectra of a PPF/AB/TiO<sub>2</sub>(1.0)/Au junction with an applied bias. Spectra progress from top to bottom, with the applied bias as indicated. The spectra are weaker than those of NAB, resulting in lower signal-to-noise ratio. All spectra have the same intensity scale, but are displaced vertically for clarity. Spectra c–e are from a different sample than a–b.

NAB/TiO<sub>2</sub> case, as shown in Fig. 3. AB is a weaker Raman scatterer than NAB, so a more transparent 1.0 nm TiO<sub>2</sub> layer was used instead of 3.0 nm. Spectra of a PPF/AB/TiO<sub>2</sub>(1.0)/Au junction are shown in Fig. 8. As expected, the bands for the NO<sub>2</sub> stretch (1340 cm<sup>-1</sup>) and phenyl–NO<sub>2</sub> stretch (1108 cm<sup>-1</sup>) are absent. However, AB exhibits a partially reversible loss of intensity under negative bias, similar to that observed for PPF/NAB(4.5)/TiO<sub>2</sub>(1.0)/Au and PPF/NAB(4.5)/TiO<sub>2</sub>(3.0)/Au junctions. The Raman intensity increases further over the bottom spectrum of Fig. 8 if the potential is returned to +3 V. We conclude that a NO<sub>2</sub> group is not a requirement for the bias induced reduction of either NAB or AB, nor is it required for the junction to exhibit rectification.

## Discussion

The principal experimental observations which bear on the mechanism of junction behavior are as follows: First, the NAB/AlO<sub>x</sub> and NAB/TiO<sub>2</sub> junctions exhibit bias-induced structural changes, with the Raman spectra following a sufficiently negative voltage excursion (PPF negative) corresponding to those of electrochemically reduced NAB. Second, AlO<sub>x</sub> and TiO<sub>2</sub> junctions are much less conductive than Cu junctions, with AlO<sub>x</sub> junctions having low conductance over the entire ±3 V range examined. However, NAB/TiO<sub>2</sub> junctions exhibit differential conductance (*dI/dV*) approximately equal to that of Cu for voltages greater than 2.5 V. Third, the reduction of NAB or AB for negative bias accompanies rectification in the TiO<sub>2</sub> junctions. These two examples do not establish a cause and effect relationship between reduction and rectification, but they do provide a correlation. Finally, the nitro group of NAB is not required to observe rectification, and azobenzene shows spectral and electronic characteristics which are qualitatively similar to those of NAB.

A possible rationale for explaining the observations is based on the vacuum referenced energy levels shown in Figs. 9 and 10. AlO<sub>x</sub> and TiO<sub>2</sub> constitute barriers to electron transfer, but with energetically different heights. In the absence of an oxide, ET through the PPF/NAB/Cu junction is rapid, leading to the high current intensities for Cu junctions (Figs. 3 and 4). As noted elsewhere, this ET is due to coherent or diffusive tunneling, and its weak temperature dependence implies negligible structural rearrangement and accompanying nuclear motion.<sup>34,48</sup> Furthermore, although the current through Cu junctions is strongly dependent on molecular structure (Fig. 2), the current densities are all much higher than those observed with oxide junctions. With an AlO<sub>x</sub> layer present, electrons cannot pass through the junction, and are presumably blocked by the oxide layer. Although the dc current through NAB/AlO<sub>x</sub> junctions is more than three orders of magnitude smaller than that for Cu junctions, the Raman results still indicate that NAB is reduced under

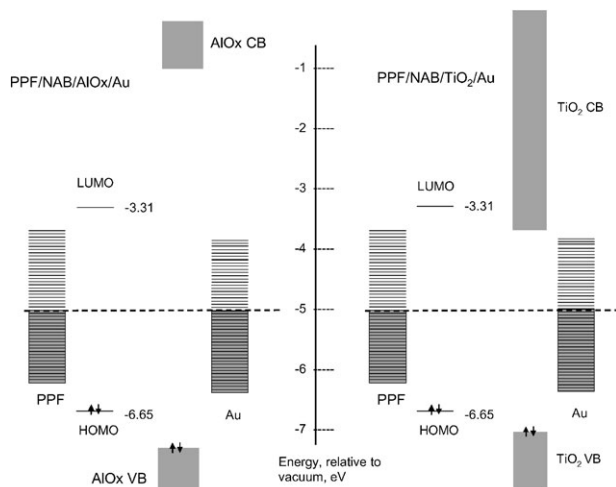


**Fig. 9** Vacuum referenced energy levels for NAB, TiO<sub>2</sub>, and AlO<sub>x</sub>. NAB orbital energies calculated from Gaussian 98. Levels shown are for isolated materials, before junction formation.

negative bias in the AlO<sub>x</sub> junction. Apparently, the high electric field across the NAB layer is acting like the ionic double layer in electrochemical reduction, by providing the driving force for injection of an electron from the PPF to the NAB. Electrical double layers in electrochemical cells are typically  $10^5$ – $10^6$  V cm<sup>-1</sup>, while the field calculated for a PPF/NAB(4.5)/AlO<sub>x</sub>(3.3)/Au(7.0) junction is  $4 \times 10^6$  V cm<sup>-1</sup> at -3 V. This estimate assumes a linear potential profile between the PPF and Au, but even higher electric fields are possible if the potential profile is nonlinear.

The behavior of the NAB/TiO<sub>2</sub> junction is similar to that of NAB/AlO<sub>x</sub> for  $(-1 < V < 1$  V), yielding similar, featureless  $J/V$  curves in this region (Fig. 4). Positive bias across a PPF/NAB/TiO<sub>2</sub>/Au junction raises the Fermi level of the Au, as shown in the right side of Fig. 10. For low positive bias, the electrons in the Au have insufficient energy to reach the TiO<sub>2</sub> conduction band, and the junction current is small, similar to the NAB/AlO<sub>x</sub> case. For higher positive bias, the electrons in Au can pass through the conduction band and the NAB LUMO, resulting in a large increase in current. Under this postulate, the conductance should approach that for the Cu junction once the TiO<sub>2</sub>

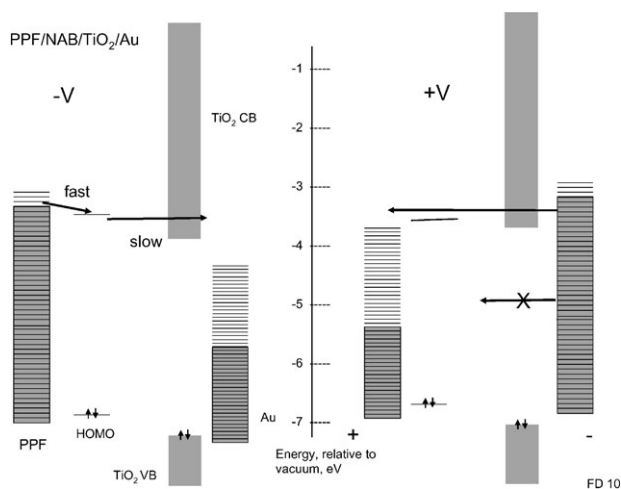
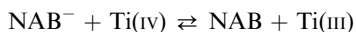


**Fig. 10** Postulated effects of applied bias on energy levels and electron transport in PPF/NAB(4.5)/TiO<sub>2</sub>/Au junctions. Arrows indicate electron transport between phases for negative (left) and positive (right) bias.

conduction band is reached. The similarity of the  $dI/dV$  slopes for NAB/Cu and NAB/TiO<sub>2</sub> above +2 V indicates that the TiO<sub>2</sub> conduction band is contributing very little resistance in the bias range above +2 V. When a negative bias is applied to the NAB/TiO<sub>2</sub> junction, the NAB is reduced, presumably because the electron cannot pass across the TiO<sub>2</sub> band gap. The electron is likely to be injected into the NAB layer just as it was with NAB/AlO<sub>x</sub>, but apparently it spends long enough in the NAB layer to permit nuclear rearrangement and NAB reduction. Rectification may result from formation of a Coulomb blockade by the anionic NAB. It is also possible that reduction causes changes in the LUMO energy, which inhibit conduction.

As noted above, an alternative explanation for conductance changes is based on a completed redox cell, in which both NAB and TiO<sub>2</sub> undergo redox reactions. For example, a cell reaction such as:



could change the conductance of both the Ti and NAB layers as well as produce the observed Raman changes, with a positive bias driving the reaction to the right and a negative bias driving it to the left. The distinction between a capacitor, which reduces NAB by an electric field, and a conventional redox cell lies in the role of possible counterions. If residual water or reaction products are present in a completed junction, it is conceivable that ions may move between the organic and oxide layers. In addition, a counter reaction at the Au electrode is necessary for charge balance in a conventional redox cell. Such ions and counter reactions are currently undetermined, if present at all, and would require Au oxidation in the case of PPF/NAB/AlO<sub>x</sub>/Au junctions. If adventitious counterions are absent, then the NAB reduction is caused by a large imposed electric field, and the “counterion” is actually the image charge formed on the Au electrode. If counterion motion is involved, it is possible that reduced NAB is stabilized by an unknown cation, possibly H<sup>+</sup>. Stated differently, the molecular junctions containing Ti or Al oxide may be acting as small capacitors or small batteries, with possible counterion motion determining the electric field distribution through the junction. In either case, the spectroscopic results unequivocally establish that structural changes occur in the molecular layer in response to an applied electric field.

Two phenomena discussed here may have general significance to molecular junctions which do not involve a carbon substrate. First, metal oxides may play a role in junction behavior, either by undergoing redox chemistry or by forming an insulating phase. UHV conditions are required to deposit Al or Ti without forming oxides, and AlO<sub>x</sub> has been identified previously as a factor in metal/molecule/metal tunnel junctions.<sup>56,57</sup> Furthermore, Ti has two oxidation states between Ti(0) and Ti(IV), which can undergo redox reactions and/or participate in the semiconducting properties of TiO<sub>2</sub>. Second, the metal oxides can retard or completely prevent electron transport through the junction, thereby imposing a large electric field across the molecular layer. In the present example, the AlO<sub>x</sub> and TiO<sub>2</sub> layers brought about the reduction of NAB, whereas the more highly conducting Cu did not. The combination of NAB and TiO<sub>2</sub> resulted in rectification, which did not occur if either phase was absent.<sup>30–32</sup> Finally, it is clear that the behavior of molecular junctions depends on the identity and properties of both the molecular layer and the “contacts”, whether they involve metal oxides or not.

## Acknowledgements

This work was supported by ZettaCore, Inc., and by the National Science Foundation through project 0211693 from the Analytical and Surface Chemistry Division.

## References

- 1 J. Jortner and M. Ratner, *Molecular Electronics*, Blackwell Science Ltd., Oxford, 1997.
- 2 C. R. Kagan and M. A. Ratner, *MRS Bull.*, 2004, 376.
- 3 A. Nitzan and M. A. Ratner, *Science*, 2003, **300**, 1384.
- 4 R. McCreery, *Chem. Mater.*, 2004, **16**, 4477.
- 5 R. McCreery, *Interface*, 2004, **13**, 46.
- 6 G. Leatherman, E. N. Durantini, D. Gust, T. A. Moore, A. L. Moore, S. Stone, Z. Zhou, P. Rez, Y. Z. Li and S. M. Lindsay, *J. Phys. Chem. B*, 1999, **103**, 4006.
- 7 S. N. Yaliraki, A. E. Roitberg, C. Gonzalez, V. Mujica and M. A. Ratner, *J. Phys. Chem.*, 1999, **111**, 6997.

- 8 S. M. Lindsay, *Interface*, 2004, **13**.
- 9 A. M. Rawlett, T. J. Hopson, L. A. Nagahara, R. K. Tsui, G. K. Ramachandran and S. M. Lindsay, *Appl. Phys. Lett.*, 2002, **81**, 3043.
- 10 G. K. Ramachandran, J. K. Tomfohr, O. F. Sankey, J. Li, X. Zarate, A. Primak, Y. Terazano, T. A. Moore, A. L. Moore, D. Gust, L. A. Nagahara and S. M. Lindsay, *J. Phys. Chem. B*, 2003, **107**, 6162.
- 11 J. He, F. Chen, J. Li, O. Sankey, Y. Terazono, C. Herrero, D. Gust, T. Moore, A. L. Moore and S. M. Lindsay, *J. Am. Chem. Soc.*, 2005, **127**, 1384.
- 12 R. J. Hamers, S. K. Coulter, M. D. Ellison, J. S. Hovis, D. F. Padowitz, M. P. Schwartz, C. M. Greenliet and J. N. Russell, Jr., *Acc. Chem. Res.*, 2000, **33**, 617.
- 13 S. K. Coulter, M. P. Schwartz and R. J. Hamers, *J. Phys. Chem. B*, 2001, **105**, 3079.
- 14 L. Fang, J. Liu, S. Coulter, X. Cao, M. P. Schwartz, C. Hacker and R. J. Hamers, *Surf. Sci.*, 2002, **514**, 362.
- 15 C. Zhou, M. R. Deshpande, M. A. Reed, L. Jones and J. M. Tour, *Appl. Phys. Lett.*, 1997, **71**, 611.
- 16 F. Anariba and R. L. McCreery, *J. Phys. Chem. B*, 2002, **106**, 10355.
- 17 P. Lewis, C. Inman, Y. Yao, J. Tour, J. Hutchinson and P. Weiss, *J. Am. Chem. Soc.*, 2004, **126**, 12214.
- 18 L. T. Cai, H. Skulason, J. G. Kushmerick, S. K. Pollack, J. Naciri, R. Shashidhar, D. L. Allara, T. E. Mallouk and T. S. Mayer, *J. Phys. Chem. B*, 2004, **108**, 2827.
- 19 J. J. Stapleton, P. Harder, T. A. Daniel, M. D. Reinard, Y. Yao, D. W. Price, J. M. Tour and D. L. Allara, *Langmuir*, 2003, **19**, 8245.
- 20 J. Chen, W. Wang, M. A. Reed, A. M. Rawlett, D. W. Price and J. M. Tour, *Appl. Phys. Lett.*, 2000, **77**, 1224.
- 21 J. M. Seminario, A. G. Zacarias and J. M. Tour, *J. Am. Chem. Soc.*, 1999, **121**, 411.
- 22 J. R. Heath and M. A. Ratner, *Phys. Today*, 2003, **56**, 43.
- 23 C. P. Collier, J. O. Jeppesen, Y. Luo, J. Perkins, E. W. Wong, J. R. Heath and J. F. Stoddart, *J. Am. Chem. Soc.*, 2001, **123**, 12632.
- 24 C. P. Collier, G. Mattersteig, E. W. Wong, Y. Luo, K. Beverly, J. Sampaio, F. M. Raymo, J. F. Stoddart and J. R. Heath, *Science*, 2000, **289**, 1172.
- 25 R. M. Metzger, J. W. Baldwin, W. J. Shumate, I. R. Peterson, P. Mani, G. J. Mankey, T. Morris, G. Szulczewski, S. Bosi, M. Prato, A. Comito and Y. Rubin, *J. Phys. Chem. B*, 2003, **107**, 1021.
- 26 R. M. Metzger, *Chem. Rev.*, 2003, **103**, 3803.
- 27 R. M. Metzger, T. Xu and I. R. Peterson, *J. Phys. Chem. B*, 2001, **105**, 7280.
- 28 S. Ranganathan, I. Steidel, F. Anariba and R. L. McCreery, *Nano Lett.*, 2001, **1**, 491.
- 29 A. O. Solak, S. Ranganathan, T. Itoh and R. L. McCreery, *Electrochem. Solid State Lett.*, 2002, **5**, E43.
- 30 R. L. McCreery, J. Dieringer, A. O. Solak, B. Snyder, A. Nowak, W. R. McGovern and S. DuVall, *J. Am. Chem. Soc.*, 2003, **125**, 10748.
- 31 R. McCreery, J. Dieringer, A. O. Solak, B. Snyder, A. M. Nowak, W. R. McGovern and S. DuVall, *J. Am. Chem. Soc.*, 2004, **126**, 6200.
- 32 A. Nowak and R. McCreery, *J. Am. Chem. Soc.*, 2004, **126**, 16621.
- 33 A. M. Nowak and R. L. McCreery, *Anal. Chem.*, 2004, **76**, 1089.
- 34 F. Anariba, J. Steach and R. McCreery, *J. Phys. Chem. B*, 2005, **109**, 11163.
- 35 S. Ranganathan, *Preparation Modification and Characterization of a Novel Carbon Electrode Material for Applications in Electrochemistry and Molecular Electronics*, PhD Thesis, Ohio State University, 2001.
- 36 S. Ranganathan and R. L. McCreery, *Anal. Chem.*, 2001, **73**, 893.
- 37 J. K. Kariuki and M. T. McDermott, *Langmuir*, 2001, **17**, 5947.
- 38 J. K. Kariuki and M. T. McDermott, *Langmuir*, 1999, **15**, 6534.
- 39 C. Combella, F. Kanoufi, J. Pinson and F. Podvorica, *Langmuir*, 2005, **21**, 280.
- 40 K. Boukerma, M. M. Chehimi, J. Pinson and C. Blomfield, *Langmuir*, 2003, **19**, 6333.
- 41 E. Coulon, J. Pinson, J.-D. Bourzat, A. Commercon and J.-P. Pulicani, *Langmuir*, 2002, **17**, 7102.
- 42 M. Delamar, G. Desarmot, O. Fagebaume, R. Hitmi, J. Pinson and J. Saveant, *Carbon*, 1997, **35**, 801.
- 43 P. Allongue, M. Delamar, B. Desbat, O. Fagebaume, R. Hitmi, J. Pinson and J. M. Saveant, *J. Am. Chem. Soc.*, 1997, **119**, 201.
- 44 P. A. Brooksby and A. J. Downard, *Langmuir*, 2004, **20**, 5038.
- 45 B. Ortiz, C. Saby, G. Y. Champagne and D. Belanger, *J. Electroanal. Chem.*, 1998, **455**, 75.
- 46 F. Anariba, S. H. DuVall and R. L. McCreery, *Anal. Chem.*, 2003, **75**, 3837.
- 47 A. J. Downard, *Langmuir*, 2000, **16**, 9680.
- 48 W. R. McGovern, F. Anariba and R. McCreery, *J. Electrochem. Soc.*, 2005, **152**, E176.
- 49 R. J. Kalakodimi, A. M. Nowak and R. McCreery, *Chem. Mater.*, 2005, DOI: 10.1012/cm050689c.
- 50 J. D. Ramsey, S. Ranganathan, J. Zhao and R. L. McCreery, *Appl. Spectrosc.*, 2001, **55**, 767.
- 51 T. Itoh and R. L. McCreery, *J. Am. Chem. Soc.*, 2002, **124**, 10894.
- 52 A. Cyr, P. Huot, G. Belot and J. Lessard, *Electrochim. Acta*, 1990, **35**, 147.
- 53 G. Seshadri and J. A. Kelber, *J. Electrochem. Soc.*, 1999, **146**, 3762.
- 54 T. Umehayashi, T. Yamaki, H. Itoh and K. Asai, *Appl. Phys. Lett.*, 2002, **81**.
- 55 J. Portier, G. Campet, C. Kwon, J. Etourneau and M. Subramanian, *Int. J. Inorg. Mater.*, 2001, **3**, 1091.
- 56 J. J. Hoagland, X. D. Wang and K. W. Hipps, *Chem. Mater.*, 1993, **5**, 54.
- 57 J. J. Hoagland, J. Dowdy and K. W. Hipps, *J. Phys. Chem.*, 1991, **95**, 2246.